Impacts of the Madden–Julian Oscillation on the Summer South China Sea Ocean Circulation and Temperature

GUIHUA WANG AND ZHENG LING

State Key Laboratory of Satellite Ocean Environment Dynamics, Second Institute of Oceanography, State Oceanic Administration, Hangzhou, China

RENGUANG WU

Institute of Space and Earth Information Science and Department of Physics, The Chinese University of Hong Kong, Hong Kong, China

CHANGLIN CHEN

State Key Laboratory of Satellite Ocean Environment Dynamics, Second Institute of Oceanography, State Oceanic Administration, Hangzhou, China

(Manuscript received 11 November 2012, in final form 8 April 2013)

ABSTRACT

The present study investigates the impact of the Madden–Julian oscillation (MJO) on the South China Sea (SCS) in summer with three types of models: a theoretical Sverdrup model, a 1.5-layer reduced gravity model, and a regional ocean model [Regional Ocean Modeling System (ROMS)]. Results show that the ocean circulation in the SCS has an intraseasonal oscillation responding to the MJO. During its westerly phase, the MJO produces positive (negative) wind stress curl over the northern (southern) SCS and thus induces an enhanced cyclonic (anticyclonic) circulation in the northern (southern) SCS. This not only cools sea surface temperature (SST) but also decreases (increases) subsurface temperature in the northern (southern) SCS. During its easterly phase, the MJO basically produces a reversed but weaker influence on SCS ocean circulation and temperature. Thus, the MJO can have an imprint on the summer climatology of SCS circulation and temperature. The authors' analysis further indicates that the MJO's dynamic effect associated with wind is generally more important than its thermodynamic effect in modulating the regional ocean circulation and temperature. The present study suggests that the MJO is important for summer ocean circulation and temperature in the SCS.

1. Introduction

The Madden–Julian oscillation (MJO) is the dominant tropical intraseasonal signal with periods of 20–90 days (Madden and Julian 1994; Zhang 2005). It is characterized by atmospheric circulation and moist convection anomalies that propagate eastward from the Indian Ocean to the western Pacific. The MJO can influence rainfall in many regions, modulating the weather systems and interacting with the ocean (Jones et al. 1998; Maloney and Hartmann 2000; Morita et al. 2006; Han et al. 2006, 2007; Huang et al. 2011).

The South China Sea (SCS) is a unique semienclosed ocean basin with potentially strong links to the MJO. The upper-layer circulation in the SCS is mainly determined by regional winds, with additional influences from the Kuroshio in the northern part of the SCS (Su 2004). Under the influence of the East Asian monsoon, a basinwide cyclonic circulation prevails in winter, whereas the summer circulation features a cyclonic gyre and an anticyclonic gyre in the northern and southern SCS, respectively (Xu et al. 1982; Liu et al. 2001; also see Fig. 1). Previous studies have demonstrated that both the tropical cyclone and thermocline circulation can contribute to the SCS upper-layer circulation (Wang et al. 2009; Wang et al. 2012). However,

Corresponding author address: Guihua Wang, Second Institute of Oceanography, State Ocean Administration, Baochubei Road 36, Hangzhou 310012, China.
E-mail: guihua_wanggh@yahoo.com.cn

DOI: 10.1175/JCLI-D-12-00796.1

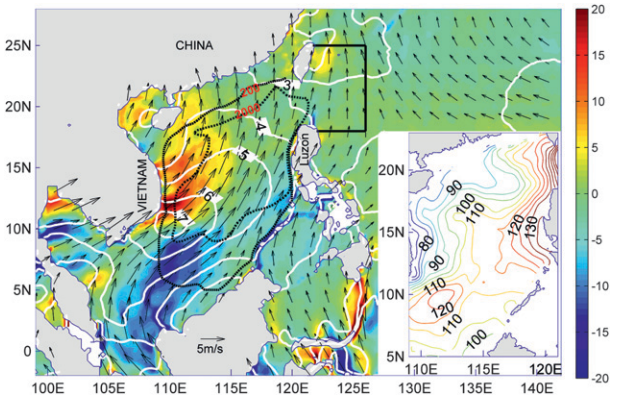

FIG. 1. Summer mean surface wind vector (black arrows), wind stress curl (color shading; 10^{-8} N m^{-3}), and wind speed (white contour; m s^{-1}). The two black contours are for 200- and 2000-m isobaths. Black lines at 18° and 24.5°N are open boundaries for the reduced gravity model, while the south, north, and east boundaries in ROMS are set at 2°S, 28°N, and 142°E, respectively. Inset map shows the SCS isotherm depth (m) of 20°C from GDEM.

there is still a big gap between model simulated and observed SCS upper-layer circulation, suggesting plausible contributions from other processes.

Several recent studies have shown that summer sea surface temperature (SST), chlorophyll, and sea surface height in the SCS exhibit considerable intraseasonal variability (Gao and Zhou 2002; Isoguchi and Kawamura 2006; Xie et al. 2007; Wu 2010). Xie et al. (2007) suggested that the ocean intraseasonal events in summer are responses to atmospheric intraseasonal wind oscillations. Since the strongest MJO occurs north of the equator and propagates from the Bay of Bengal to the SCS in summer, it is very likely that the atmospheric MJO can affect the SCS summer ocean circulation. The purpose of the present paper is to investigate the effects of the MJO on summer ocean circulation in the SCS by using observational data and three numerical models: a theoretical model, a reduced gravity model, and a regional ocean model [Regional Ocean Modeling System (ROMS)]. Unless otherwise specified below, the MJO refers to the atmospheric oscillation and the SCS oscillation refers to the ocean response.

2. Data

The wind data used in this study are Quick Scatterometer (QuikSCAT) wind (Mostovoi et al. 2006) from the National Aeronautics and Space Administration (NASA). The spatial resolution is 0.25° latitude by 0.25° longitude, and the time period is from 2000 to 2007. For the purpose of studying the MJO influence on ocean circulation, a 20–90-day bandpass filter is applied to extract the MJO from the original wind. Two wind forcings are used to drive the ocean models: the unfiltered wind and the wind excluding the MJO.

The air–sea net heat flux data are the daily objectively analyzed air–sea fluxes (OAFlux; Yu and Weller 2007) product from Woods Hole Oceanographic Institution (WHOI). The spatial resolution is 1° latitude by 1° longitude, and the time period is from 2000 to 2007. As with the wind data, a 20–90-day bandpass filter is applied to extract the MJO from the original heat flux. Two heat fluxes are constructed: the unfiltered heat flux and the heat flux excluding the MJO.

The sea surface height anomaly (SSHA) dataset of the U.S. Navy Modular Ocean Data Assimilation System (MODAS) is a merged product (Jacobs et al. 2002) from all available altimeter missions [Ocean Topography Experiment (TOPEX)/Poseidon, *Jason-1*, *European Remote Sensing Satellite-1* (*ERS-1*), *ERS-2*, and *Envisat*]. The spatial resolution is 0.25° latitude by 0.25° longitude, and the temporal resolution is daily. This dataset spans the time period from 1993 to 2008. The SST dataset from January 2000 to December 2007 is also produced by the MODAS. This merged product is based on measurements by both the infrared sensors from the Moderate Resolution Imaging Spectroradiometer (MODIS) and microwave sensors from Advanced Microwave Scanning Radiometer for Earth Observing System (AMSR-E) and the Tropical Rainfall Measuring Mission (TRMM) Microwave Imager (TMI). The spatial resolution of this product is 25 km, and the temporal sampling frequency is daily.

The MJO index proposed by Wheeler and Hendon (2004) is adopted in the present analysis. This index is based on the first two empirical orthogonal functions (EOFs) of the combined fields of 850-hPa zonal wind, 200-hPa zonal wind, and outgoing longwave radiation in the equatorial region [the Real-time Multivariate MJO series (RMM); the first mode is RMM1 and the second mode is RMM2]. Because the second mode describes the atmospheric condition when the MJO produces enhanced convection over the Pacific Ocean and low-level westerlies develop over the SCS in summer, this mode is used in the present study unless otherwise specified.

3. Models

a. Sverdrup theoretical model

The Sverdrup theory is a primary balance for the large-scale wind-driven ocean circulation (Sverdrup 1947). Many studies have applied this theory to understand the SCS circulation (Metzger and Hurlburt 1996; Shaw et al. 1999; Liu et al. 2001). The wind-driven transport streamfunction ψ for flow integrated in the entire water column can be estimated by the Sverdrup theory as

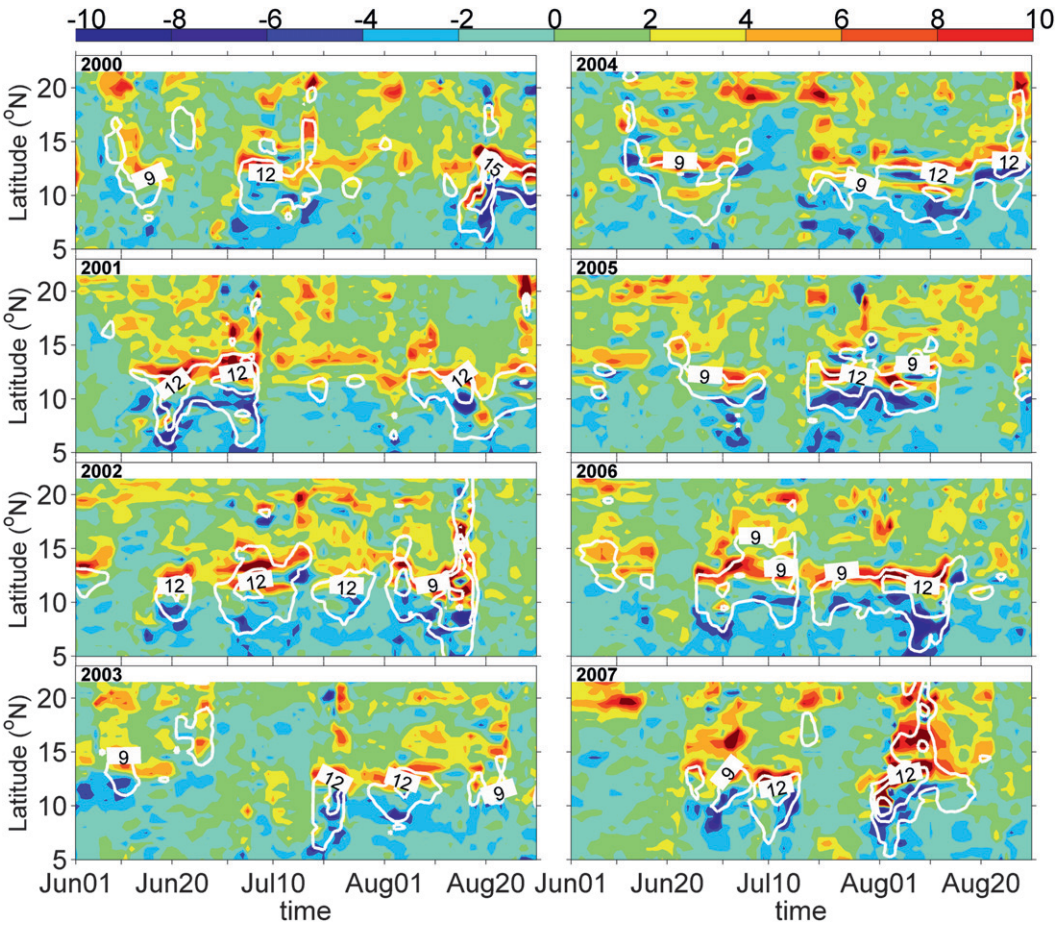

FIG. 2. Time–latitude sections of summer surface wind speed (white contour; $m\,s^{-1}$) and wind stress curl (shading color; $10^{-8}\,N\,m^{-3}$) along 111°E from 2000 to 2007.

$$\psi(x) = -\frac{1}{\rho\beta}\int_{x}^{x_E} \mathrm{curl}(\tau)\,dx,$$

where ρ is the density of the water, β is the northward gradient of the planetary vorticity, τ is the wind stress, and x_E represents the ocean eastern boundary. The boundary condition is $\psi = 0$ at x_E.

b. 1.5-layer model

A 1.5-layer nonlinear reduced gravity model is applied to simulate the wind-driven upper ocean circulation. The model boundary is set along the 200-m isobaths (Fig. 1). The reduced gravity is set to $0.03\,m\,s^{-2}$, with a lateral friction coefficient of $500\,m^2\,s^{-1}$ and an initial thermocline depth of 200 m. The model resolution is 0.25° latitude by 0.25° longitude. The model is spun up with the winds switched on gradually from the rest to the wind distribution of 1 January 2000 over a 1-month period. The model is then integrated with the wind forcing data of the whole year from 1 January to 31 December 2000. The model run is repeated for 4 yr until the ocean circulation reaches a quasi-equilibrium state. Then, the model is forced from 1 January 2000 to 31 December 2007 with the two wind forcings: the unfiltered wind and the wind excluding the MJO. More details of this simple model are discussed in Wang et al. (2006, 2008, 2009). The summer mean is defined as the average of the daily model output from 1 June to 31 August.

c. ROMS

Three-dimensional ROMS is the family of terrain-following vertical coordinate models (Shchepetkin and McWilliams 2005). The model domain extends from 2°S to 28°N and from 99° to 142°E, as shown in Fig. 1. The horizontal resolution is 1/12°. There are 30 levels in the vertical direction and a stretching method of the vertical grid is used to increase resolution near the surface and bottom boundaries (Shchepetkin and McWilliams 2009). The topography is extracted from 2-minute gridded elevations/bathymetry for the world

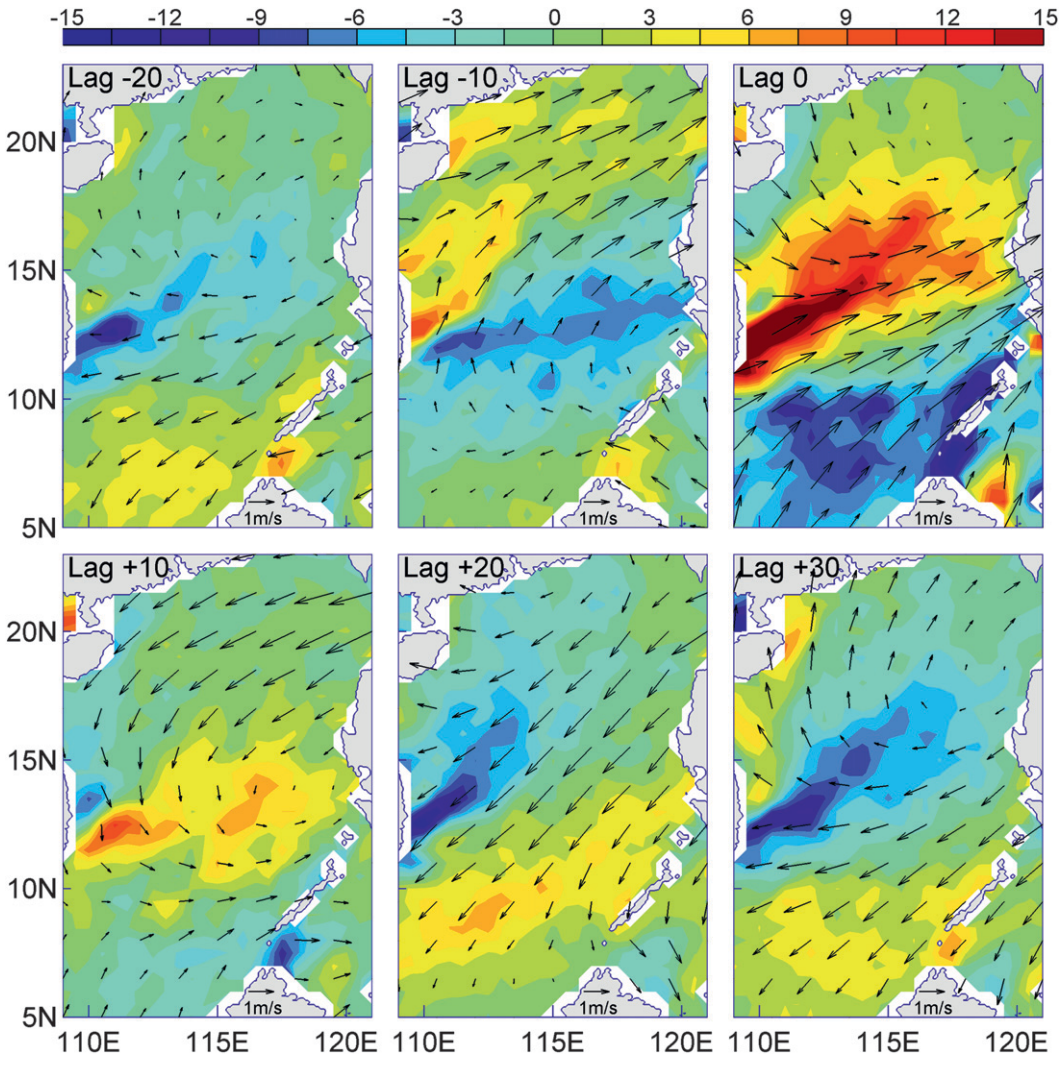

FIG. 3. Lagged regression maps between the MJO index and surface wind in increments of 10 days. Lags (days) are shown above each panel, and negative lag means MJO leads wind. Shading color is for wind stress (10^{-8} N m^{-3}), and black arrows are for wind vectors.

(ETOPO2; 1/30°) data from the U.S. National Geophysical Data Center. The initial velocities and surface elevation are set to zero, and temperature and salinity are set to the Generalized Digital Environment Model (GDEM; Carnes 2009) climatology in January. For open boundaries, radiation and no-gradient conditions are used for velocities and surface elevation, respectively (Marchesiello et al. 2001). A nonslip condition is applied to wall boundaries. Sea surface salinity is restored to the GDEM monthly climatology at a time scale of 60 days. Previous studies have shown that ROMS simulates the SCS circulation well (e.g., Gan et al. 2009; Xiu and Chai 2011).

To reach the quasi equilibrium state, the ROMS model is firstly integrated for 20 yr with monthly climatological OAFlux heat fluxes and QuikSCAT winds. Then, the model is forced from 1 January 2000 to 31 December 2007 with the four sets of daily forcings as follows:

1) the original QuikSCAT wind and OAFlux dataset;
2) both wind and heat fluxes but all excluding MJO;
3) original OAFlux and the wind excluding MJO; and
4) original wind and OAFlux excluding MJO.

4. Results

a. MJO influence on surface forcings

In summer, southwesterly winds prevail over the SCS. The climatology of wind speed shows a strong wind jet over central SCS due to orographic blockage (Fig. 1; also

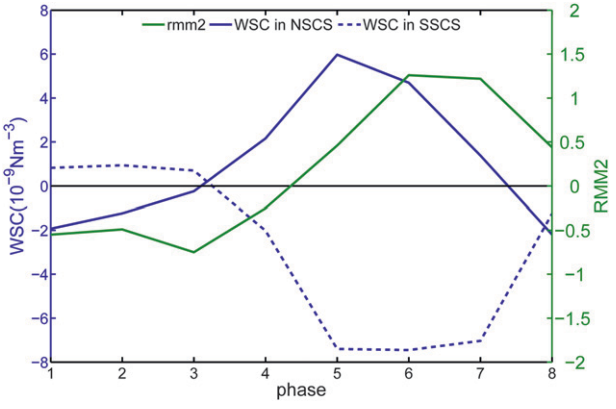

FIG. 4. Time series of the MJO index (green line) and wind stress curl (10^{-9} N m^{-3}) in the northern South China Sea (solid blue line) and in the southern South China Sea (dashed blue line) in summer.

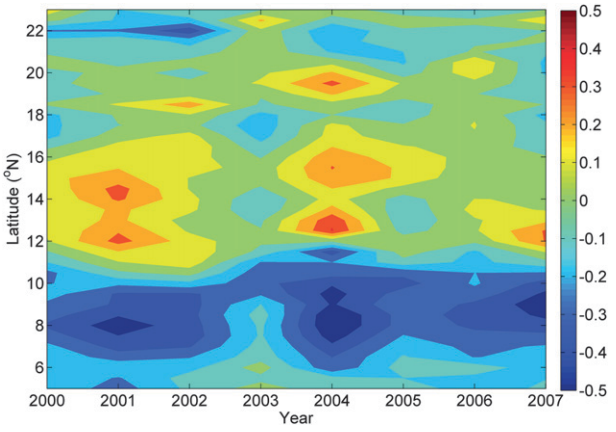

FIG. 5. The zonally averaged wind stress curl (10^{-8} N m^{-3}) induced by the MJO in each summer from 2000 to 2007.

see Xie et al. 2003). As a result, there is a positive wind stress curl over northern SCS and a negative wind stress curl over southern SCS. The time–latitude section of wind speed along 111°E shows obvious intraseasonal events associated with wind pulses each year (Fig. 2). As the wind speed becomes stronger, both the positive wind stress curl over the northern SCS and negative wind stress curl over the southern SCS become stronger, indicating robust intraseasonal oscillations in the wind stress curl.

To examine the temporal evolution of wind stress curls induced by the MJO, Fig. 3 shows the regression maps of QuikSCAT winds upon the RMM2 during eight summers from 2000 to 2007. North of 10°N, the wind anomaly is anticyclonic at lags of −20 days (MJO leading wind by 20 days), inducing a negative wind stress curl. As the MJO propagates eastward, the negative wind stress curl moves to the southern SCS gradually. Once the MJO is over the SCS (there is no lag between the MJO and SCS wind), wind anomalies become cyclonic, resulting in a strong positive wind stress curl over the northern SCS. Afterward, the positive wind stress curl gradually moves to the south SCS and the negative curl dominates the northern SCS again. South of 10°N, the wind stress curl pattern generally mirrors that to the north of 10°N.

The MJO and SCS wind stress curl oscillations can be divided into eight phases based on the first two EOF modes (RMM1 and RMM2), as proposed by Wheeler and Hendon (2004). As shown in Fig. 4, the wind stress curl over the SCS induced by MJO is not symmetric, although the MJO is an almost symmetric oscillation. The MJO affects the wind stress curl over the SCS more strongly in the westerly phase than in the easterly phase (Fig. 4), producing more positive wind stress curl over northern SCS and negative wind stress curl over southern SCS in the whole MJO period. The asymmetric wind oscillation may be associated with the behavior of MJO propagation and SCS location relative to the strongest MJO signals near the equator (Lau and Chan 1986). Figure 5 shows the zonal average of summer mean wind stress curl induced by the MJO from 2000 to 2007. Although the wind stress curl induced by the MJO over the SCS has strong interannual variability at a period of around 3 yr, the MJO generally can induce positive and negative wind stress curls to the north and south of 11°N in each summer, respectively. This further indicates that the MJO over the SCS is stronger in the westerly phase than in the easterly phase. Thus, it can enhance the summer wind stress curl over both the southern and northern SCS.

To investigate the MJO influence on heat fluxes, the regression maps of net heat flux upon the RMM2 are shown in Fig. 6. The patterns of net heat flux induced by MJO demonstrate a robust oscillation associated with wind speed. As the MJO leads wind by 20 days, the wind is intensified north and weakened south of 10°N, producing positive and negative net heat flux anomalies over the northern and southern SCS, respectively. Then, such a pattern gradually moves to the southern SCS as the MJO propagates eastward, and a reversed pattern occurs shortly before a new MJO oscillation comes. It is worth noting that the net heat flux is also affected more strongly in the westerly phase than in the easterly phase (figure is omitted).

b. Ocean circulation response to MJO

To examine the ocean adjustment processes in response to the MJO forcings, we display in Fig. 7 the regression maps of available daily satellite MODAS SSHA upon the RMM2. Because the time for the first baroclinic Rossby wave to cross the SCS basin is

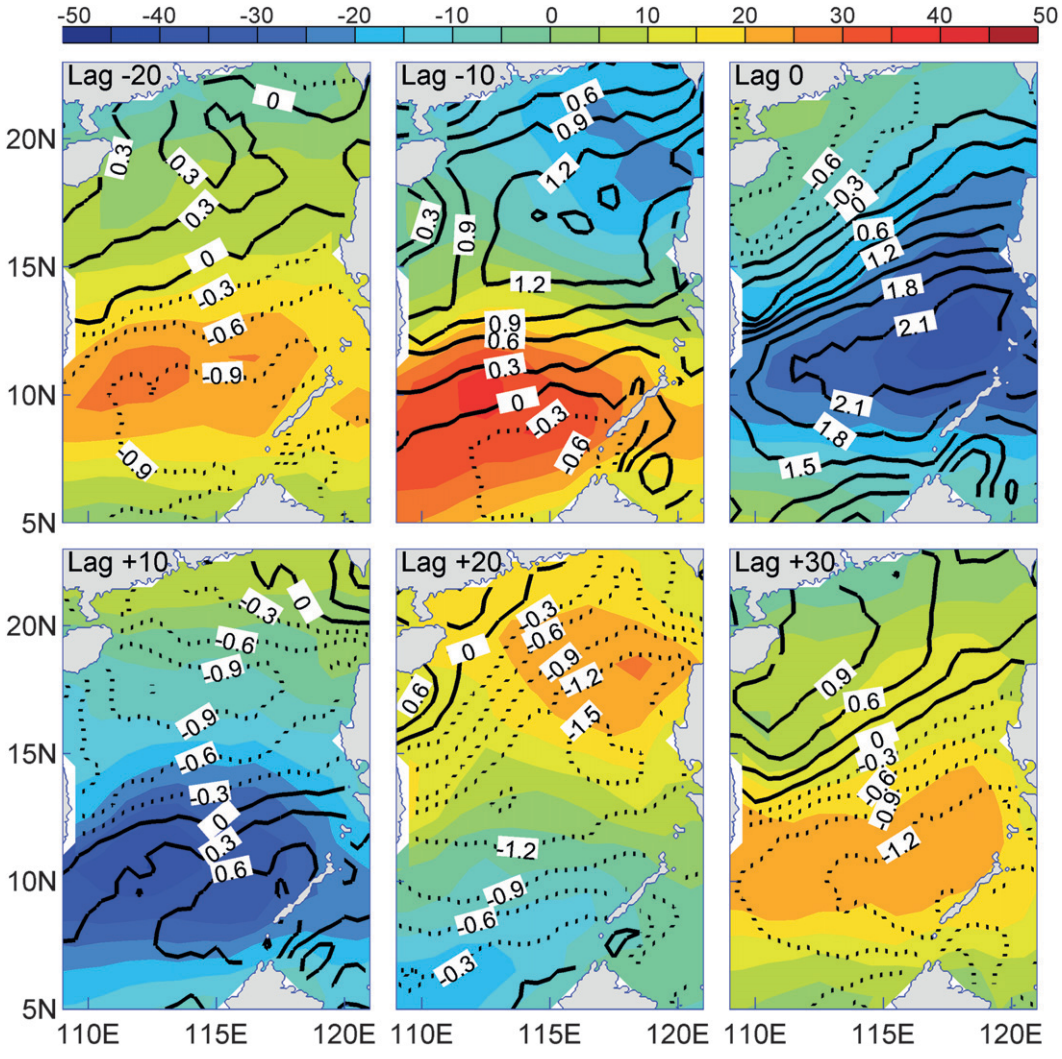

FIG. 6. Lagged regression maps between the MJO index and net heat flux in increments of 10 days. Lags (days) are shown above each panel, and negative lag means MJO leads wind. Shading color is for net heat flux ($W m^{-2}$), and black lines are for wind speed anomaly induced by MJO.

approximately 40–50 days, we display the regression maps with the SSHA lagging the wind at about 40 days. As the wind stress curl induced by the MJO is positive (negative) over the northern (southern) SCS at lag = 0 (during the MJO westerly phase), the simulated SSHA displays a cyclonic (anticyclonic) circulation anomaly in the northern (southern) SCS at lag = +40 days. In contrast, there are anticyclonic (cyclonic) circulation anomalies in the northern (southern) SCS at lag = +60 days, 40 days after (during the MJO easterly phase) the positive (negative) wind stress curl moves to the southern (northern) SCS at lag = +20 days.

Since the wind stress curl over the SCS induced by the MJO is stronger in the westerly phase than in the easterly phase, it is necessary to discuss the net effect of the MJO on the SCS ocean climatology. Figures 8a–c (top) show the summer mean streamfunction obtained from Sverdrup theory, thermocline depth from the reduced gravity model, and 20°C isotherm depth from ROMS, respectively. All of these demonstrate the large-scale summer circulation: a cyclonic gyre in the northern SCS and an anticyclonic gyre in the southern SCS are formed in response to the summer wind stress curl (Qu 2000; Liu et al. 2001; Wang et al. 2006). Compared with the Sverdrup streamfunction (Fig. 8a, top), both the thermocline depth (Fig. 8b, top) and the 20°C isotherm depth (Fig. 8c, top) display mesoscale circulations featuring a dipole structure off the coast of central Vietnam: a cyclonic eddy in the northern part and an anticyclonic eddy in the southern part. Both the simulated large-scale

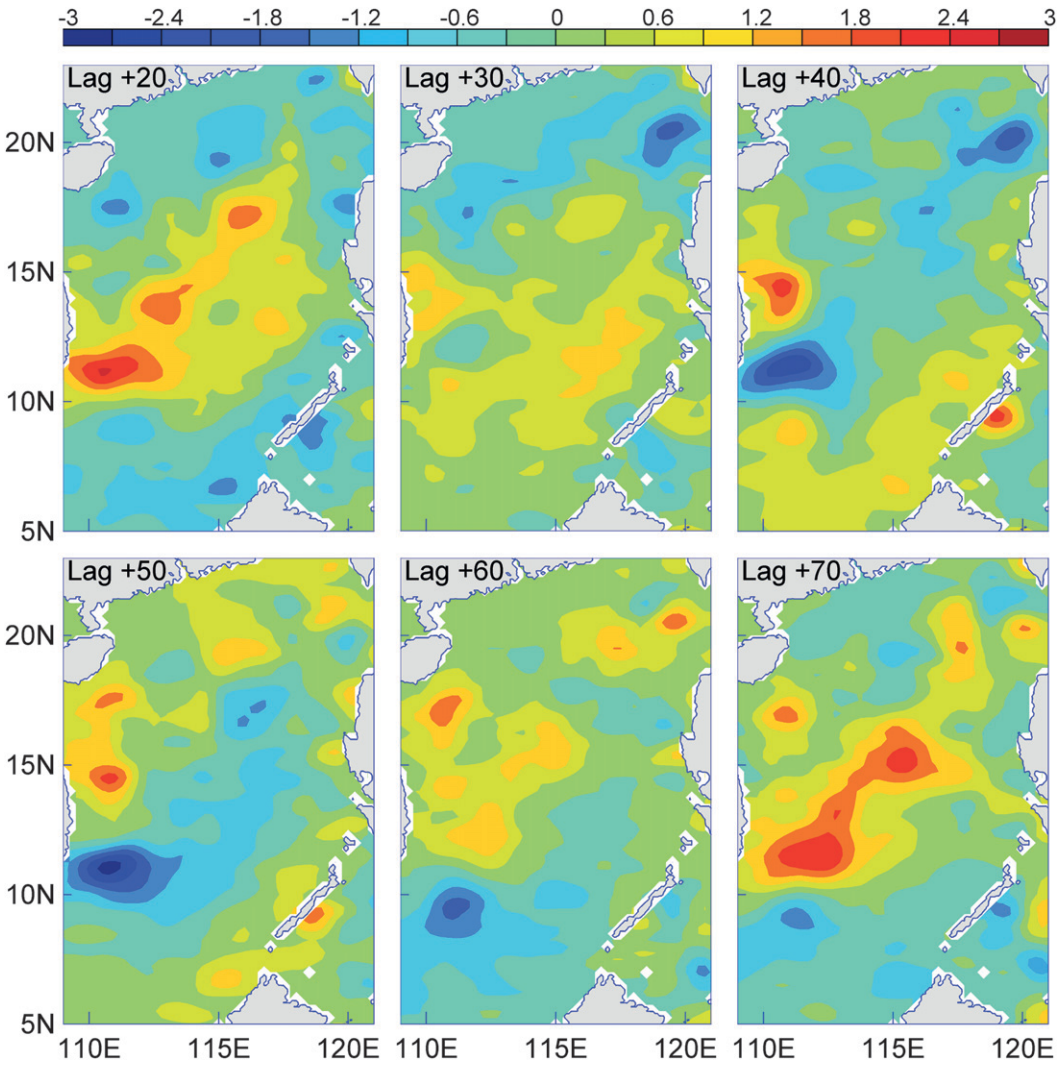

FIG. 7. Lagged regression maps between the MJO and the depth (m) of MODAS SSHA in increments of 10 days. Lags (days) are shown above each panel.

circulation and the dipole structure in the two models are in agreement with observations (the observed counterpart of the 20°C isotherm depth can be seen in Fig. 1), giving us confidence in using the three models to simulate the SCS circulation.

To consider the MJO effects on the SCS circulation climatology in summer, the three models are also driven with surface forcings without the MJO. Figures 8a–c (middle) display the simulated streamfunction, thermocline depth, and 20°C isotherm depth, respectively. Generally, the circulation patterns forced with and without the MJO are very similar. The modeled circulation differences between the original forcings and the forcings without MJO are displayed in Figs. 8a–c (bottom). The cyclonic circulation in northern SCS and the anticyclonic circulation in southern SCS are intensified when the MJO forcings are included. Accompanying the intensified gyres, the dipole off the coast of central Vietnam is strengthened in both the thermocline depth and the isotherm depth of 20°C (Figs. 8b,c, bottom). This suggests that the MJO can enhance the summer SCS circulation.

To explore the relative roles of wind and net heat flux in modulating the SCS circulation, Fig. 9a (Fig. 9b) shows the simulated SCS summer circulation differences between the original forcings and those without MJO wind forcing (net heat flux forcing). Comparing Fig. 9a with Fig. 8c, the enhanced summer large-scale circulation shown in Fig. 8c contributes largely to the MJO-induced wind stress curl. Note that the enhanced circulation contributes to the westerly phase of MJO. The circulation pattern induced by the net heat flux associated with MJO shows a robust anticyclonic circulation in the

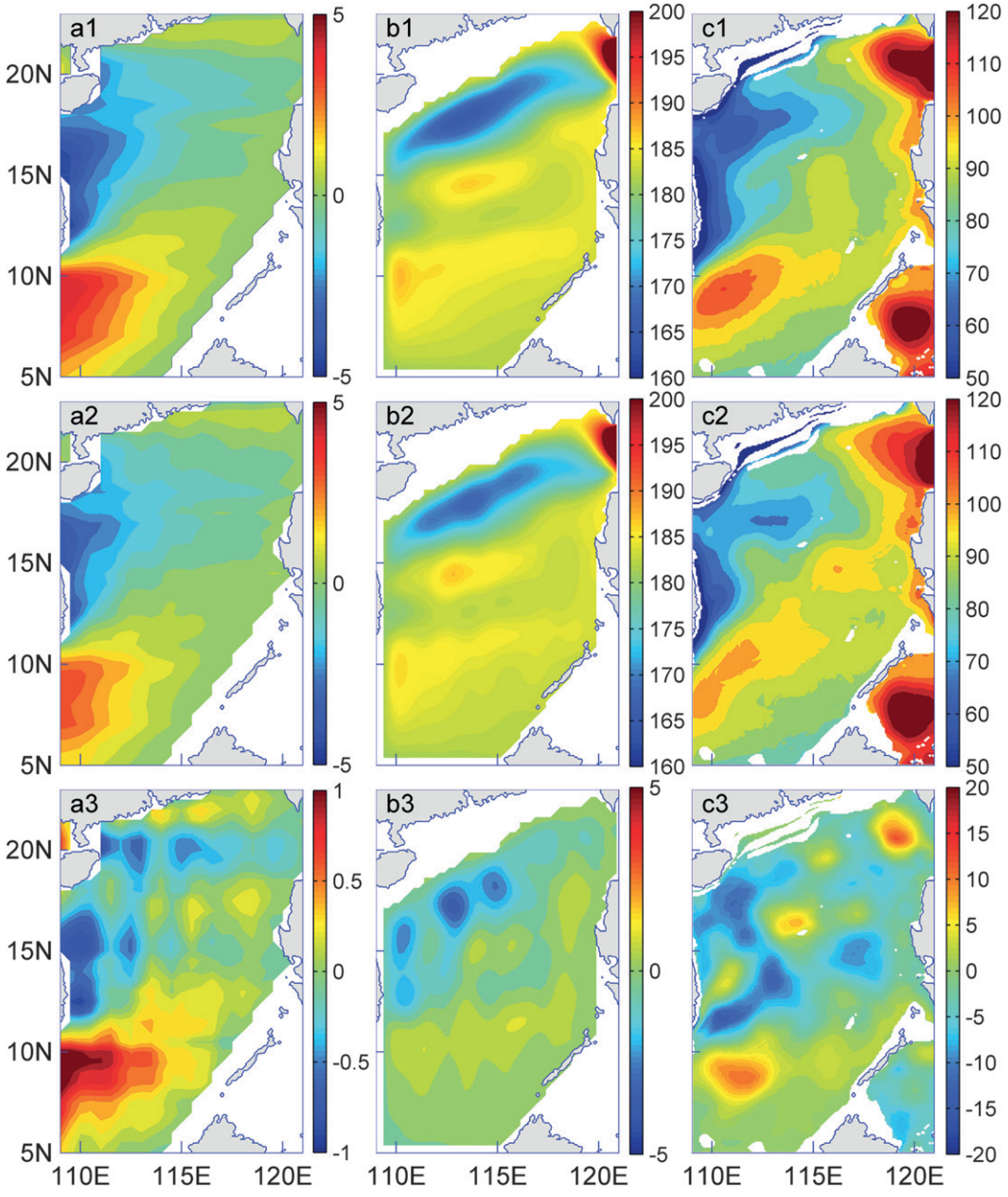

FIG. 8. Summer mean SCS circulation: (a) Sverdrup streamfunction (Sv; $1\,\text{Sv} \equiv 10^6\,\text{m}^3\,\text{s}^{-1}$), (b) thermocline depth (m) from the reduced gravity model, and (c) 20°C isotherm depth (m) from ROMS. Shown are the surface forcings that are (top) unfiltered and (middle) filtered to exclude the MJO. (bottom) The difference between (top) and (middle).

northwestern SCS and a cyclonic circulation in the southern SCS. Further analysis shows that the circulation induced by the net heat flux associated with the MJO is consistent with the estimated steric sea surface induced by the MJO (Fig. 10c), demonstrating that the steric effect has an important contribution to the circulation induced by the MJO heat flux signal. Note the steric sea surface is derived from the density change in the SCS mixed layer with the method of Gill and Niller (1973). Generally, these experiments suggest that the dynamic effect associated with wind in the MJO is more important in modulating the SCS circulation than the thermal dynamic part, although the latter also contributes.

c. *Ocean temperature response to MJO*

Temperature change likely accompanies changes of ocean dynamics and thermodynamics. Thus, it is worthy to discuss how the MJO influences the SCS temperature. Not

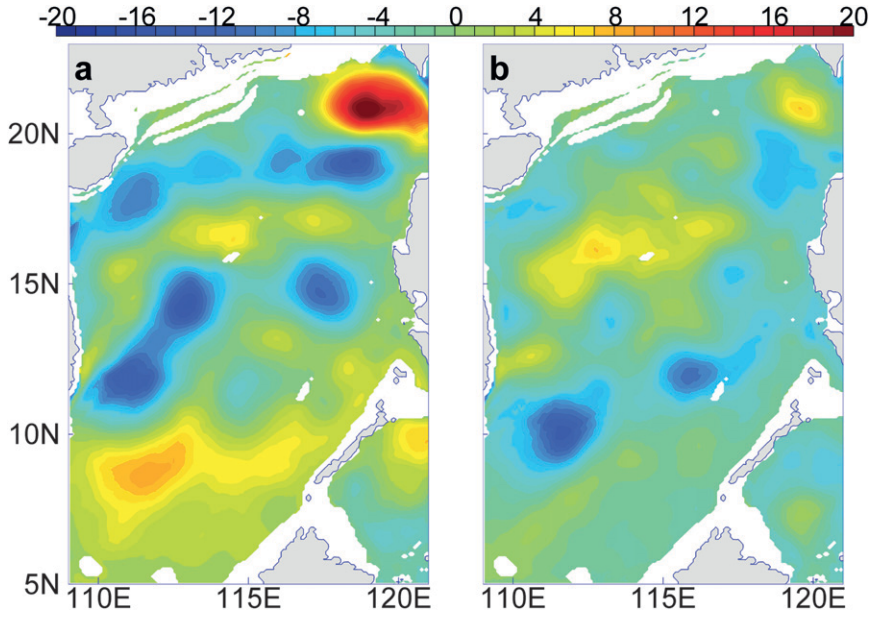

FIG. 9. The 20°C isotherm depth (m) difference from ROMS between unfiltered surface forcing and surface forcing filtered to exclude the MJO: (a) only wind and (b) only net heat flux.

unexpectedly, the MJO can induce a similar oscillation in SST as shown in Fig. 11, which has been discussed in the literature (e.g., Xie et al. 2007). Here, we only discuss the roles of dynamics and thermodynamics on the summer climatology of temperature. Note that the MJO has a stronger impact on the SCS temperature in the westerly phase than in the easterly phase, and the temperature patterns shown below are mostly caused by the westerly period of MJO.

In summer, a conspicuous surface feature is a cold water patch stretching offshore from the coast in the central SCS. This feature can be seen in the simulation from ROMS with unfiltered forcings (Figs. 12a). Compared with the simulated SST with forcings excluding the MJO, the simulated SST with unfiltered forcings is generally lower than that of MJO-excluded forcings in the whole basin (Fig. 12b). The different contributions of wind and net heat flux associated with the MJO in modulating the SCS surface temperature can be found in Figs. 12c,d, respectively. Generally, the southwesterly winds over the SCS are intensified during MJO westerly

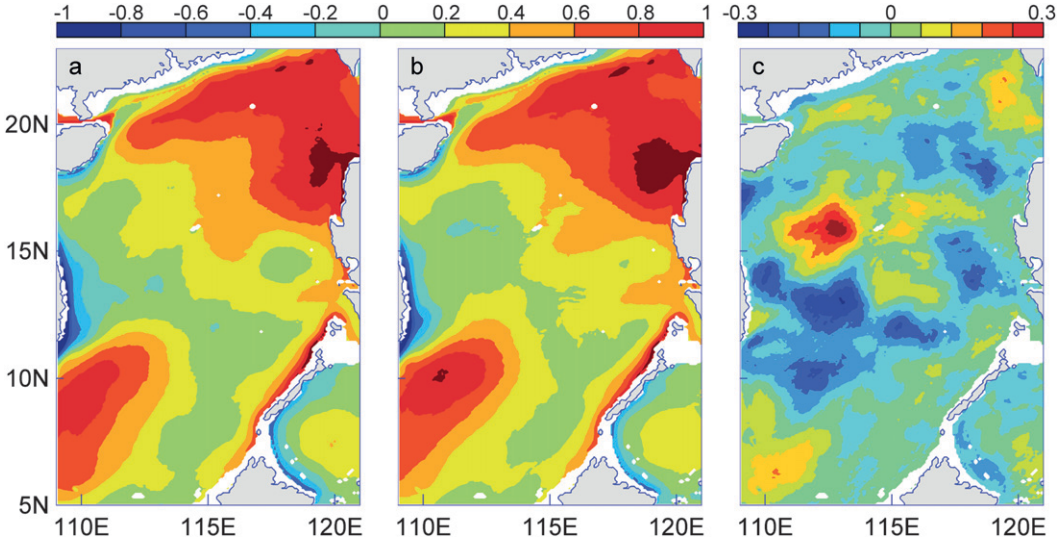

FIG. 10. The steric height anomaly (cm) from ROMS: for (a) the unfiltered net heat surface flux forcing, (b) the surface forcing filtered to exclude the MJO, and (c) the difference between (a),(b).

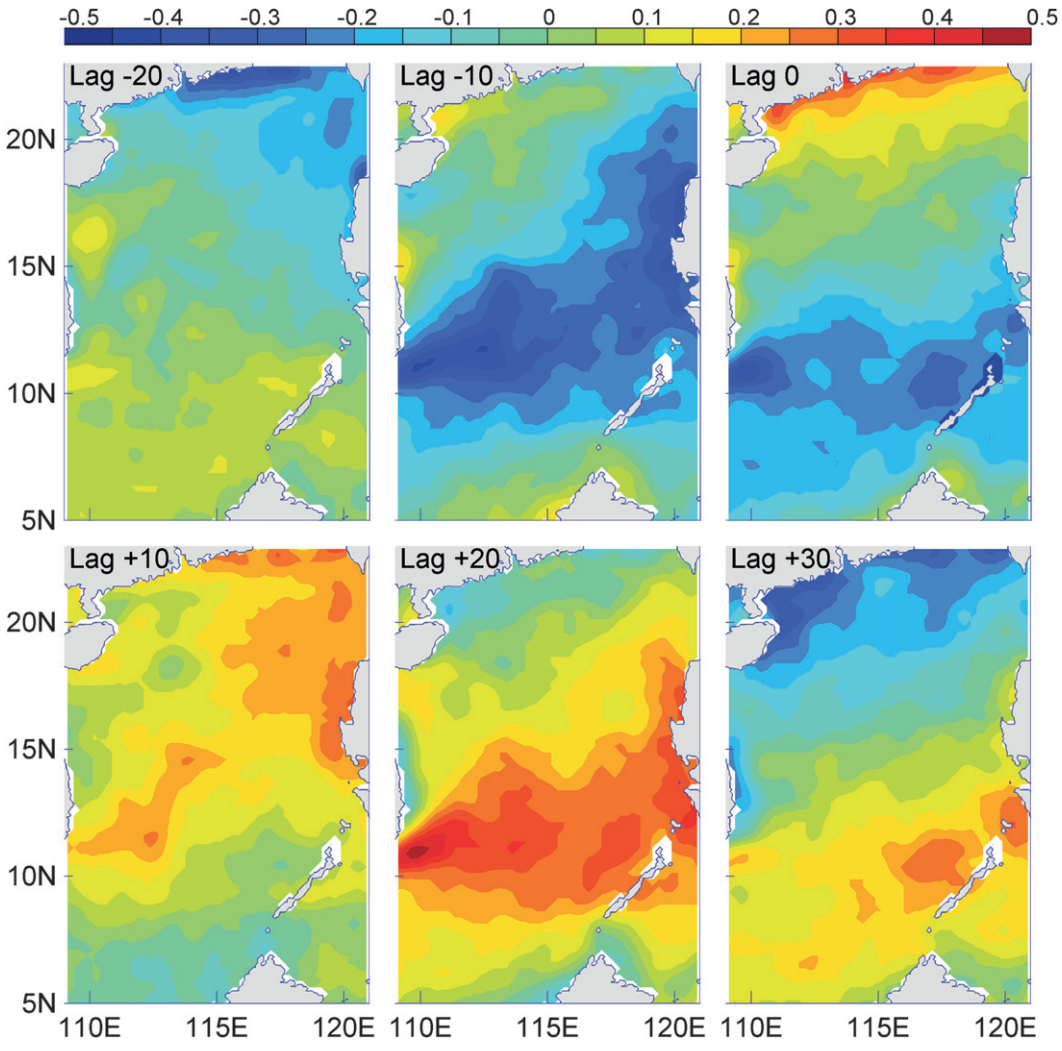

FIG. 11. Lagged regression maps between the MJO and the sea surface temperature (°C) in increments of 10 days. Lags (days) are shown above each panel.

periods, and the SST displays a basinwide cooling in response to the wind intensification, probably by entrainment cooling processes. The MJO can also input heat into the northern SCS and take out heat from the southern SCS (Fig. 12d), thus inducing positive and negative SST anomalies in the northern and southern SCS, respectively. Comparing Figs. 12c,d with Fig. 12b, the effects of winds dominate the SST variability, whereas the heat flux induced by the MJO can affect the amplitude of SST variability slightly. The dominant role of winds on SST is similar to the case in the Indian Ocean (Han et al. 2007).

The response of the temperature at 100 m to the MJO is different from the SST field. Figure 13a shows the simulated temperature at 100 m with the original forcings. From the figure, the temperature at 100 m is lower in the northern SCS than in southern SCS, which corresponds to the basinwide cyclonic circulation in the northern SCS and anticyclonic circulation in the southern SCS, respectively. The temperature differences between the original forcings and the three experiments excluding the MJO are shown in Figs. 13b–d. The simulated temperature in the northern (southern) SCS with unfiltered forcing is generally lower (higher) than that of MJO-excluded forcing (Fig. 13b). Comparing the dynamic and thermodynamic effects, the temperature change induced by the MJO appears to be mostly contributed by the wind forcing (Fig. 13c), while the net heat flux induced by MJO generally warms and cools subsurface temperature in the northern and southern SCS, respectively. These differences extend down to 400 m. The temperature change in the subsurface layers associated with the MJO may be due to the Ekman pumping (Fig. 3). The

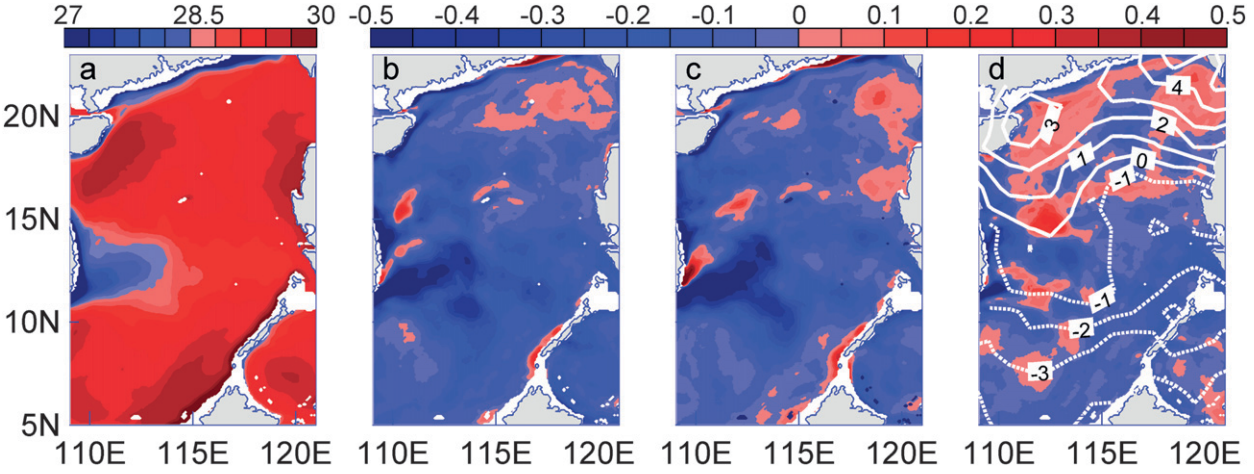

FIG. 12. Summer mean SCS sea surface temperature (°C): (a) ROMS simulation with unfiltered forcing; (b) difference between the unfiltered forcings simulation and that of MJO-excluded wind and net heat flux; (c) difference between the unfiltered forcings simulation and that of MJO-excluded wind; and (d) difference between the unfiltered forcings simulation and that of MJO-excluded net heat flux. In (d), the solid (dashed) lines are positive (negative) summer mean net heat flux ($W\,m^{-2}$) induced by the MJO.

MJO westerly phase intensifies positive wind stress curl and negative wind stress curl over the northern and southern SCS, respectively, leading to a stronger Ekman upwelling (downwelling) in the northern (southern) SCS. In response to the change in the Ekman upwelling (downwelling), the temperature in the subsurface layers in the northern (southern) SCS with unfiltered wind is generally lower (higher) than that of the MJO-excluded wind.

5. Summary and discussion

The MJO is a planetary-scale disturbance that propagates eastward from the Indian Ocean to the western Pacific Ocean through the SCS. The MJO has been shown to have a strong impact on the summer southwesterly winds over the SCS. Both observations and simulations with a theoretical model, reduced gravity model, and ROMS demonstrate that the SCS has a large response to the MJO.

The SCS circulation shows a strong response to the MJO forcings. Our analysis further suggests that the dynamic effect associated with wind field is generally more important than its thermodynamic effect in modulating the regional ocean circulation and temperature. During the westerly phase, both the positive wind stress curl over the northern SCS and the negative wind stress curl over the southern SCS are intensified, producing a stronger cyclonic gyre in the northern SCS and an

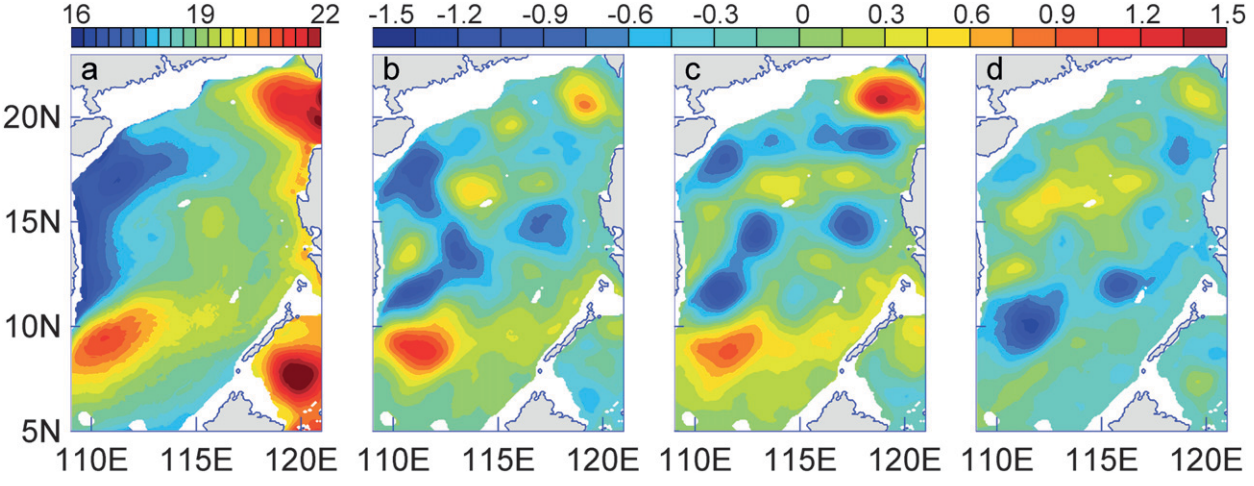

FIG. 13. Summer mean SCS temperature (°C) at 100 m: (a) ROMS simulation with unfiltered forcing; (b) difference between the unfiltered forcings simulation and that of MJO-excluded wind and net heat flux; (c) difference between the unfiltered forcings simulation and that of MJO-excluded wind; and (d) difference between the unfiltered forcings simulation and that of MJO-excluded net heat flux.

anticyclonic gyre in the southern SCS, respectively. The easterly MJO phase basically produces a reversed but weaker ocean response. Thus, the MJO can enhance the summer climatology of the SCS circulation. To estimate the contribution of the MJO-induced circulation, we calculated the ratio between the MJO-induced summer thermocline depth variance and the magnitude of the summer thermocline depth variance. The results indicate that the MJO can contribute about 9% and 16% to the variance in the northern and southern SCS, respectively.

The MJO can also induce an intraseasonal variation in the SCS temperature. Because the westerly phase of MJO has stronger effects on SCS temperature than the easterly phase, the MJO produces a temperature anomaly pattern similar to that in the westerly phase. The SST generally cools in the whole basin because the wind speed is intensified by the MJO, and the subsurface temperature is cooler (warmer) in the northern (southern) SCS associated with the ocean circulation enhanced by the MJO. Our results suggest that the dynamic effects associated with winds dominate the temperature variability, while the thermodynamic effects have some impacts on the amplitude of the SCS SST variability.

This study proposes that the MJO is an important forcing to the summer SCS circulation and its intraseasonal variation. Other scientists suggest that the instraseasonal variation of the Pacific or the Kuroshio can also propagate into the SCS (Li et al. 2007). Further investigation is necessary to distinguish the two types of intraseasonal variations in the future.

Acknowledgments. This study was supported by the National Science Foundation of China (NSFC) for Distinguished Young Scholars (41125019), National Basic Research Program of China (2012CB955601, 2013CB430301), and Natural Science Foundation of Zhejiang for Innovative Research Groups (2009R50044). RW acknowledges the support of a Hong Kong Research Grants Council grant (CUHK403612) and National Natural Science Foundation of China grants (41275081 and 41228006). Comments from Dr. Nat Johnson improved this manuscript presentation. We thank the editor and anonymous reviewers for their comments on this paper.

REFERENCES

Carnes, M. R., 2009: Description and evaluation of GDEM-V3.0. Naval Research Laboratory Rep. NRL/MR/7330-09-9165, 21 pp.

Gan, J., A. Cheung, X. Guo, and L. Li, 2009: Intensified upwelling over a widened shelf in the northeastern South China Sea. *J. Geophys. Res.,* **114,** C09019, doi:10.1029/2007JC004660.

Gao, R., and F. Zhou, 2002: Monsoonal characteristic revealed by intraseasonal variability of sea surface temperature. *Geophys. Res. Lett.,* **29,** doi:10.1029/2001GL014225.

Gill, A. E., and P. P. Niller, 1973: The theory of the seasonal variability in the ocean. *Deep-Sea Res.,* **20,** 141–177.

Han, W., W. T. Liu, and J. L. Lin, 2006: Impact of atmospheric submonthly oscillations on sea surface temperature of the tropical Indian Ocean. *Geophys. Res. Lett.,* **33,** L03609, doi:10.1029/2005GL025082.

——, D. Yuan, W. T. Liu, and D. J. Halkides, 2007: Intraseasonal variability of Indian Ocean sea surface temperature during boreal winter: Madden-Julian oscillation versus submonthly forcing and processes. *J. Geophys. Res.,* **112,** C04001, doi:10.1029/2006JC003791.

Huang, P., C. Chou, and R. H. Huang, 2011: Seasonal modulation of tropical intraseasonal oscillation on tropical cyclone genesis in the western North Pacific. *J. Climate,* **24,** 6339–6352.

Isoguchi, O., and H. Kawamura, 2006: MJO-related summer cooling and phytoplankton blooms in the South China Sea in recent years. *Geophys. Res. Lett.,* **33,** L16615, doi:10.1029/2006GL027046.

Jacobs, G. A., C. N. Barron, D. N. Fox, K. R. Whitmer, S. Klingenberger, D. May, and J. P. Blaha, 2002: Operational altimeter sea level products. *Oceanography,* **15,** 13–21.

Jones, C., D. E. Waliser, and C. Gautier, 1998: The influence of the Madden–Julian oscillation on ocean surface heat fluxes and sea surface temperature. *J. Climate,* **11,** 1057–1072.

Lau, K. M., and P. H. Chan, 1986: Aspects of the 40–50 day oscillation during the northern summer as inferred from outgoing longwave radiation. *Mon. Wea. Rev.,* **114,** 1354–1367.

Li, L., C. Jing, and D. Zhu, 2007: Coupling and propagating of mesoscale sea level variability between the western Pacific and the South China Sea. *Chin. Sci. Bull.,* **52,** 1699–1707, doi:10.1007/s11434-007-0203-3.

Liu, Z. Y., H. J. Yang, and Q. Y. Liu, 2001: Regional dynamics of seasonal variability in the South China Sea. *J. Phys. Oceanogr.,* **31,** 272–284.

Madden, R. A., and P. R. Julian, 1994: Detection of a 40-50 day tropical oscillation: A review. *Mon. Wea. Rev.,* **112,** 814–837.

Maloney, E. D., and D. L. Hartmann, 2000: Modulation of eastern North Pacific hurricanes by the Madden–Julian oscillation. *J. Climate,* **13,** 1451–1460.

Marchesiello, P., J. C. McWilliams, and A. Shchepetkin, 2001: Open boundary conditions for long-term integration of regional oceanic models. *Ocean Modell.,* **3,** 1–20.

Metzger, E. J., and H. Hurlburt, 1996: Coupled dynamics of the South China Sea, Sulu Sea, and the Pacific Ocean. *J. Geophys. Res.,* **101,** 12 331–12 352.

Morita, J., Y. N. Takayabu, S. Shige, and Y. Kodama, 2006: Analysis of rainfall characteristics of the Madden-Julian oscillation using TRMM satellite data. *Dyn. Atmos. Oceans,* **42,** 107–126.

Mostovoi, G. V., P. J. Fitzpatrick, and Y. Li, 2006: Regional accuracy of QuikSCAT gridded winds. *Int. J. Remote Sens.,* **26,** 4117–4136.

Qu, T. D., 2000: Upper-Layer circulation in the South China Sea. *J. Phys. Oceanogr.,* **30,** 1450–1460.

Shaw, P. T., S. Y. Chao, and L. L. Fu, 1999: Sea surface height variation in the South China Sea from satellite altimetry. *Oceanol. Acta,* **22,** 1–17.

Shchepetkin, A. F., and J. C. McWilliams, 2005: The Regional Oceanic Modeling System (ROMS): A split-explicit, free-surface,

topography-following-coordinate oceanic model. *Ocean Modell.,* **9,** 347–404.

——, and ——, 2009: Correction and commentary for ''Ocean forecasting in terrain-following coordinates: Formulation and skill assessment of the Regional Ocean Modeling System.'' *J. Comput. Phys.,* **228,** 8985–9000, doi:10.1016/j.jcp.2009.09.002.

Su, J., 2004: Overview of the South China Sea circulation and its influence on the coastal physical oceanography near the Pearl River estuary. *Cont. Shelf Res.,* **24,** 1745–1760.

Sverdrup, H. U., 1947: Wind-driven currents in a baroclinic ocean; With application to the equatorial currents of the eastern Pacific. *Proc. Natl. Acad. Sci. USA,* **33,** 318–326.

Wang, G., D. Chen, and J. Su, 2006: Generation and life cycle of the dipole in South China Sea summer circulation. *J. Geophys. Res.,* **111,** C06002, doi:10.1029/2005JC003314.

——, ——, and ——, 2008: Winter eddy genesis in the eastern South China Sea due to orographic wind jets. *J. Phys. Oceanogr.,* **38,** 726–732.

——, Z. Ling, and C. Wang, 2009: Influence of tropical cyclones on seasonal ocean circulation in the South China Sea. *J. Geophys. Res.,* **114,** C10022, doi:10.1029/2009JC005302.

——, R. X. Huang, J. Su, and D. Chen, 2012: The effects of thermohaline circulation on wind-driven circulation in the South China Sea. *J. Phys. Oceanogr.,* **42,** 2283–2296.

Wheeler, M., and H. H. Hendon, 2004: An all-season real-time multivariate MJO index: Development of an index for monitoring and prediction. *Mon. Wea. Rev.,* **132,** 1917–1932.

Wu, R., 2010: Subseasonal variability during the South China Sea summer monsoon onset. *Climate Dyn.,* **34,** 629–642.

Xie, S.-P., Q. Xie, D. Wang, and W. T. Liu, 2003: Summer upwelling in the South China Sea and its role in regional climate variations. *J. Geophys. Res.,* **108,** 3261, doi:10.1029/2003JC001867.

——, C.-H. Chang, Q. Xie, and D. Wang, 2007: Intraseasonal variability in the summer South China Sea: Wind jet, cold filament, and recirculations. *J. Geophys. Res.,* **112,** C10008, doi:10.1029/2007JC004238.

Xiu, P., and F. Chai, 2011: Modeled biogeochemical responses to mesoscale eddies in the South China Sea. *J. Geophys. Res.,* **116,** C10006, doi:10.1029/2010JC006800.

Xu, X. Z., Z. Qiu, and H. C. Chen, 1982: The general description of the horizontal circulation in the South China Sea (in Chineses). *Proc. of the 1980 Symp. on Hydrometeorology,* Beijing, China, Chinese Society of Oceanology and Limnology, 137–145.

Yu, L. S., and R. A. Weller, 2007: Objectively analyzed air–sea heat fluxes (OAFlux) for the global ice-free oceans (1981–2005). *Bull. Amer. Meteor. Soc.,* **88,** 527–539.

Zhang, C., 2005: Madden-Julian oscillation. *Rev. Geophys.,* **43,** RG2003, doi:10.1029/2004RG000158.